ADVANCED ENERGY MATERIALS
www.advenergymat.de

A Versatile Planar Building Block with C_{2V} Symmetry for High-Performance Non-Halogenated Solvent Processable Polymer Donors

Hang Wang, Hao Lu, Ya-Nan Chen, Andong Zhang, Yuqiang Liu, Dawei Li, Yahui Liu, Xinjun Xu, and Zhishan Bo**

Planar building block B2TCl with C_{2V} symmetry configuration is designed to prepare polymer donors (PB2TCl-*o* and PB2TCl-*i*) with good solubility in non-halogenated solvents. When blended with BTP-ec9-4F, PB2TCl-*o*-based devices processed by 1,2-dimethylbenzene (*o*-DMB) give a power conversion efficiency (PCE) of 15.10% with a V_{oc} of 0.89 V, a J_{sc} of 24.37 mA cm^{-2}, and an fill factor of 69.69%. Semitransparent OSCs based on PB2TCl-*o*:BTP-ec9-4 can afford a PCE of 9.09% with an average visible transmittance (AVT) of 23.9% and an AT of 24.2%. B2TCl-*o* is also used as a third component to prepare random terpolymers PW1 and PW2. Using *o*-DMB as the processing solvent, PW1 and PW2-based devices give improved PCEs of 16.26% and 17.19%, respectively, which are much higher than the parent polymers (PM6 and D18). This work provides a versatile building block B2TCl-*o* for the preparation of non-halogen solvent processable high-performance polymer donor materials.

1. Introduction

Organic solar cells (OSCs) have received a lot of attention due to their irreplaceable advantages such as light-weight, semi-transparency, mechanical flexibility, weak light response, solution processability, etc.[1–3] During past several years, mainly benefited from the development of nonfullerene acceptors such as ITIC,[4] Y6,[5] etc., the power conversion efficiency (PCE) of single-junction OSCs has reached over 18%,[6–10] which is much higher than the benchmark PCE of 15% considered as the commercialization threshold. However, there are still some issues to be solved for future application. For example, the current state-of-the-art PSCs are mostly processed with harmful halogenated solvents such as chloroform (CF), chlorobenzene (CB) and 1,2-dichlorobenzene (*o*-DCB),[11–15] which will result in the large-scale accumulation of halogen atoms and be detrimental to human health and ecosystems.[16–18] Therefore, developing high-performance non-halogenated solvent processable OSCs is of great significance for future industrial applications.[19,20]

The prerequisite of high efficiency OSCs is that the active layer should form bicontinuous interpenetrating network without severe phase separation to promote the exciton dissociation and charge transport.[21,22] As for the active layer composed by polymer donor and small molecular acceptor, the semi-crystalline polymers should preferentially aggregate during the film deposition and then the small molecules could solidify between the crystalline aggregates.[23] However, the state-of-the-art conjugated polymer donors usually suffer from limited solubilities in non-halogenated solvents, which could induce over-sized phase separation and reduced photovoltaic performance.[24,25] Hence, the polymer donor should be designed to have good solubility and processability in non-halogenated solvents. The introduction of bulky/long side chains and enhanced twisty of molecular backbone are often used to design non-halogenated solvents soluble polymer donors.[26–29] However, these molecular design strategies generally lead to reduce molecular crystallinity and packing, thus partly sacrificing the charge transport ability of the polymer.[30] All in all, the key point of high-performance non-halogenated solvent processable polymers is to balance the contradiction of crystallinity and solubility.

Herein, we design two polymer donors (PB2TCl-*o* and PB2TCl-*i*) with donor–donor (D–D) alternating molecular backbones. Compared with donor–acceptor (D–A) type polymer donor, this specific molecular structure could reduce the intramolecular charge transfer effect to achieve wide-bandgap polymer donors,[31] which can match well with typical efficient low-bandgap acceptor (BTP-ec9-4F). Moreover, this molecular design can weaken the intermolecular interactions and improve the solubility of the polymer donors. Besides, the key building blocks B2TCl-*o* and B2TCl-*i* are of C_{2V} symmetry, which can form "zig zag-shape" molecular backbone and enhance the solubility of the polymer.[32,33] In a word, these two polymers are both of non-halogenated solvents processability. Unlike B2TCl-*i*, B2TCl-*o* with Cl atoms substituted at outer-positions displays

H. Wang, Y.-N. Chen, A. Zhang, Y. Liu, Y. Liu, Z. Bo
College of Textiles & Clothing
State Key Laboratory of Bio-Fibers and Eco-Textiles
Qingdao University
Qingdao 266071, China
E-mail: liuyh@qdu.edu.cn; zsbo@bnu.edu.cn
H. Lu, D. Li, X. Xu, Z. Bo
Beijing Key Laboratory of Energy Conversion and Storage Materials
College of Chemistry
Beijing Normal University
Beijing 100875, China
The ORCID identification number(s) for the author(s) of this article can be found under https://doi.org/10.1002/aenm.202104028.

DOI: 10.1002/aenm.202104028

nearly planar molecular geometry. Hence, the photovoltaic performance of PB2TCl-*o* and PB2TCl-*i* are significantly different. Using *o*-DMB as the processing solvent, PB2TCl-*i* based devices can only afford a PCE of 0.13%; whereas PB2TCl-*o* based ones can give an impressive PCE of 15.10%. Besides, semitransparent OSCs based on PB2TCl-*o*:BTP-ec9-4F can deliver a PCE of 9.09% with an AVT of 23.9% and an AT of 24.2%. Furthermore, the building block B2TCl-*o* is also used as a third component to prepare random terpolymers (PW1 and PW2). Using *o*-DMB as processing solvent, PW1 and PW2 based devices can give PCEs of 16.26% and 17.19%, respectively, which are much higher than the parent polymers PM6 (15.16%) and D18 (16.18%). Our work demonstrate that B2TCl-*o* is a useful building block to prepare non-halogenated solvent processable polymer donors.

2. Results and Discussion

The chemical structures of polymer donors (PB2TCl-*o* and PB2TCl-*i*) and small molecular acceptor (BTP-ec9-4F) are shown in **Scheme 1**, where BTP-ec9-4F and compound **1** were prepared according to previously reported procedures.[32,34] Stille cross-coupling of compound **1** with IM1 and IM2 using $Pd(PPh_3)_4$ as the catalyst precursor and toluene as the solvent afforded compounds **2** and **5** in yields of 77% and 71%, respectively. The treatment of compound **2** with Bu_4NF to remove TIPS group afforded compound **3** in a yield of 94%. Then bromination of compounds **3** and **5** with NBS furnished compounds B2TCl-*o* and B2TCl-*i* in yields of 68% and 54%, respectively. Stille polymerization is adopted with $Pd_2(dba)_3$ and $P(o\text{-tol})_3$ as the catalyst precursors afforded the target polymer donors PB2TCl-*o* and PB2TCl-*i* in yields of 55% and 62%, respectively. These two polymers exhibit good solubility in common organic solvents, especially non-halogenated solvents such as toluene, 1,2-dimethylbenzene (*o*-DMB), 1,2,4-trimethyl benzene (TMB) etc., which provide a chance for fabricating eco-friendly photovoltaic devices. PB2TCl-*o* and PB2TCl-*i* display similar number-average molecular weight (M_n) (62.5 and 71.7 kDa) and polydispersity indexes (PDI) (2.37 and 2.36), which can avoid the influence of molecular weight and provide a better comparison.

The molecular geometries of PB2TCl-*o* and PB2TCl-*i* are estimated by density functional theory (DFT) calculations at the B3LYP/6-31G(d) level, the side chains are shortened to methoxy to simplify the calculations. As shown in the Supporting Information, the molecular backbone of the two polymers are both of "zig zag-shape" due to C_{2v} symmetry of the building blocks (B2TCl-*o* and B2TCl-*i*), which can reduce the intermolecular interactions of polymer chains and ensure good solubilities of the polymers. However, B2TCl-*o* and B2TCl-*i* display markedly different molecular geometries. As shown in **Figure 1**, B2TCl-*o* with the chlorine atom located at the outer position is nearly planar with a small dihedral angle of 15°; whereas, the inner chlorinated molecule B2TCl-*i* is twisted with a large dihedral angle of 43° due to the steric repulsion between Cl and H atoms.[35] All in all, there are three potential benefits of PB2TCl-*o*: firstly, the D–D type molecular backbone can reduce the intramolecular charge transfer and endow the polymer donor with a wide optical bandgap, which is favorable for efficient photon utilization when paired with low bandgap acceptor; secondly, the introduction of C_{2v} building block can enhance the solubility, which is conducive to the preparation of devices by eco-friendly organic solvent; thirdly, the planar polymer backbone is beneficial for the delocalization of π-electrons, the intermolecular packing, and thus higher charge transport mobility.

The UV–vis absorption behaviors of PB2TCl-*o* and PB2TCl-*i* in dilute *o*-DMB solutions at different temperature are investigated. As shown in **Figure 2**a,b, two polymers exhibit wide absorptions in the range of 400–600 nm. As for PB2TCl-*o*, two featured vibrational transition peaks (0-0 and 0-1) located at 508 and 537 nm can be observed, and the 0-0 absorption peak is gradually decreased with the increase of solution temperature,

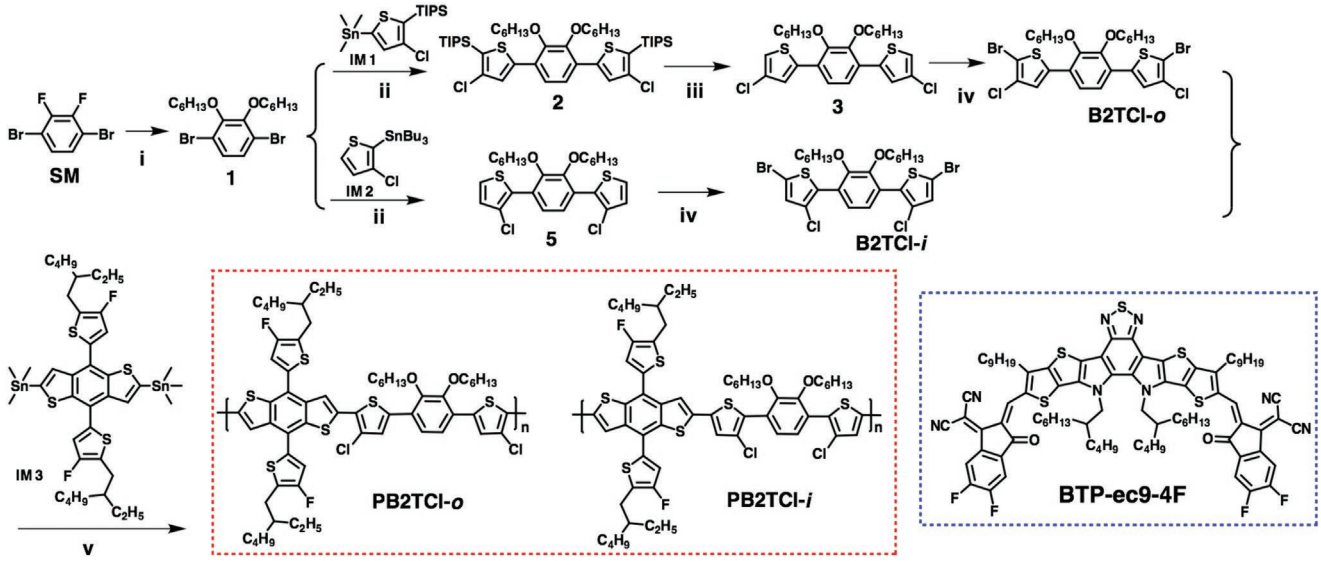

Scheme 1. The chemical structure of BTP-ec9-4F and synthetic routes of PB2TCl-*o* and PB2TCl-*i*. Conditions and reagents: i) *t*-BuOK, 1-Hexanol, THF, reflux; ii) $Pd(PPh_3)_4$, toluene, reflux; iii) Tetrabutylammonium fluoride (TBAF), THF, 0 °C; iv) NBS, $CHCl_3$, rt; v) $Pd_2(dba)_3$, $P(o\text{-tol})_3$, chlorobenzene, 140 °C.

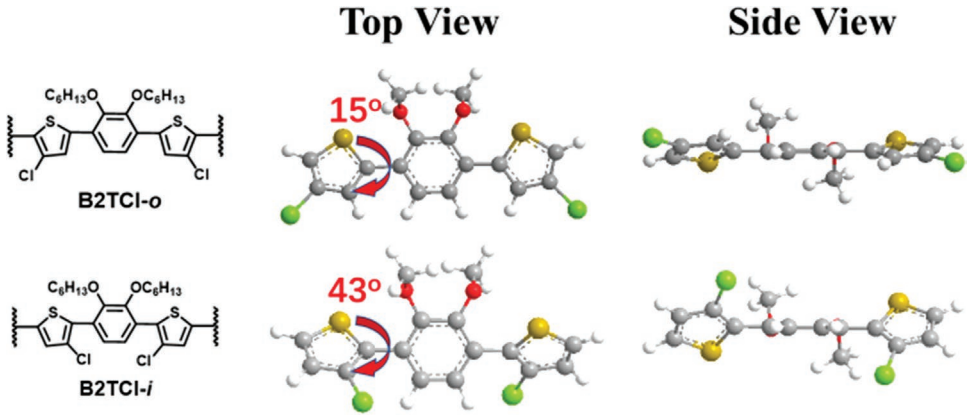

Figure 1. Optimal geometries of building block (B2TCl-*o* and B2TCl-*i*) determined by DFT.

indicating its temperature-dependent aggregation property. Unlike PB2TCl-*o*, the absorption peaks of PB2TCl-*i* are featureless and almost unchanged at elevated temperature, indicating its non-aggregated character in solution, which can be ascribed to its nonplanar molecular backbone (vide supra). In going from solutions to films, the absorption spectra of PB2TCl-*o* and PB2TCl-*i* are both red-shifted. Thanks to the D-D type molecular backbone, the optical bandgaps of PB2TCl-*o* and PB2TCl-*i* are as large as 2.16 and 2.12 eV, respectively, according to the absorption edge of thin films. The energy levels of BTP-ec9-4F, PB2TCl-*o* and PB2TCl-*i* are estimated by cyclic voltammetry (Supporting Information). According to the equation: $E_{HOMO/LUMO} = -e(E_{onset,ox/red} - E_{Fc/Fc+} + 4.80)$, the highest occupied molecular orbital (HOMO) and the lowest unoccupied molecular orbital (LUMO) energy levels are calculated to be −5.73/−3.58 eV for BTP-ec9-4F, −5.64/−3.49 eV for PB2TCl-*o* and −5.67/−3.56 eV for PB2TCl-*i*. The energy level diagram of BTP-ec9-4F, PB2TCl-*o* and PB2TCl-*i* is shown in Figure 2. The related data are also summarized in **Table 1**.

The photovoltaic performance of the as-synthesized polymers is investigated by fabricating OSCs with an inverted device configuration of ITO/PEDOT:PSS/Donor:BTP-ec9-4F/PDINN/Ag. The *J*–*V* curves and photovoltaic parameters are shown in **Figure 3** and **Table 2**, respectively. Chlorobenzene is initially used as the processing solvent, a PCE of 14.43% is achieved for PB2TCl-*o* based devices. Considering the good solubility of

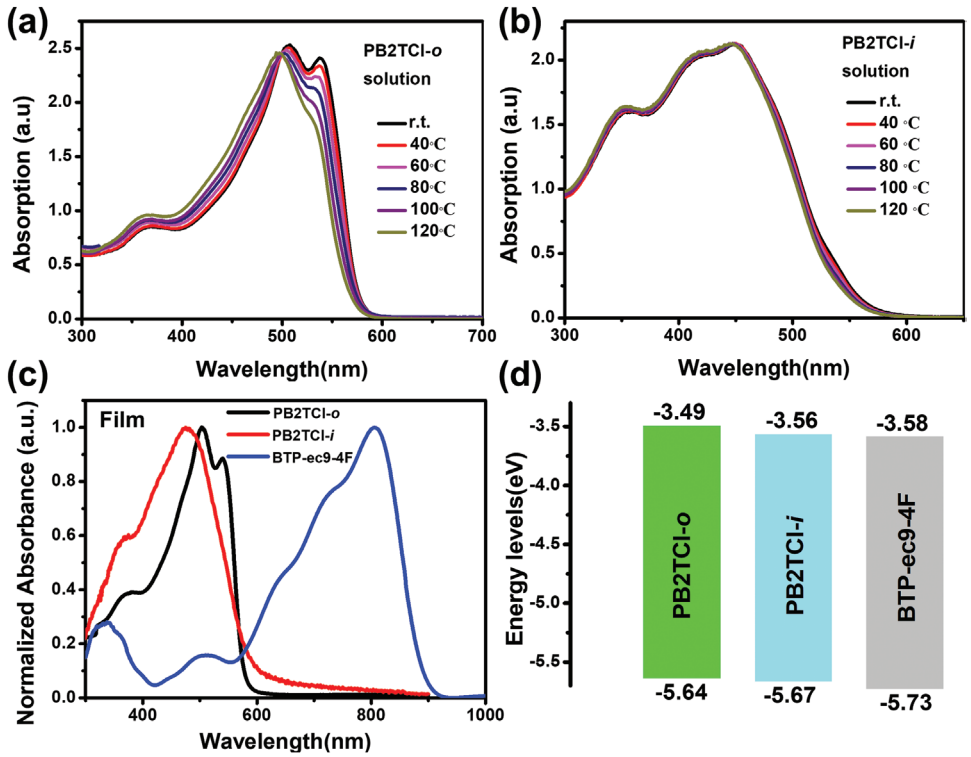

Figure 2. a,b) Normalized absorptions of PB2TCl-*o* and PB2TCl-*i* in *o*-DMB at different temperature; c) Normalized absorptions of BTP-ec9-4F, PB2TCl-*o* and PB2TCl-*i* as films; d) energy diagram of devices.

Table 1. Optical and electrochemical properties of PB2TCl-*o* and PB2TCl-*i*.

Polymer	λ_{max}[a)] [nm]	λ_{max}[b)] [nm]	E_g^{opt} [eV]	HOMO [eV]	LUMO [eV]
PB2TCl-*o*	508, 537	504, 542	2.16	−5.64	−3.49
PB2TCl-*i*	448	475	2.12	−5.67	−3.56

[a)]In dilute *o*-DMB solutions.; [b)]As thin films.

Table 2. Photovoltaic parameters of PB2TCl-*o* and PB2TCl-*i* based devices.

Active layer	V_{oc} [V]	J_{sc} [mA cm^{-2}]	FF [%]	$PCE_{max/ave}$ [%]
PB2TCl-*i*:BTP-ec9-4F[a)]	0.84	0.63	25.30	0.13
PB2TCl-*o*:BTP-ec9-4F[a)]	0.89	24.37 (23.41)[b)]	69.69	15.10 (14.95)

[a)]Processed by *o*-DMB; [b)]Calculated by EQE curve.

polymer donors, non-halogenated solvent (*o*-DMB) is used as the processing solvent to fabricate organic solar cells. Surprisingly, PB2TCl-*o* based devices give an excellent PCE of 15.10% with an open-circuit voltage (V_{oc}) of 0.89 V, a short-circuit current (J_{sc}) of 24.37 mA cm^{-2} and a fill factor (FF) of 69.69%, which is much higher than PB2TCl-*i* based ones (0.13%). The inferior charge transport mobility and large-scale phase separation are responsible for the poor photovoltaic performance of PB2TCl-*i* based devices (vide infra). To investigate the charge-transport properties, the space charge-limited current (SCLC) measurements of PB2TCl-*o* and PB2TCl-*i* based devices are performed. Hole and electron mobilities are evaluated by fabricating hole-only and electron-only devices with the device architectures of ITO/PEDOT:PSS/PB2TCl-*o*:BTP-ec9-4F/Au and ITO/ZnO/PB2TCl-*o*:BTP-ec9-4F/Al, respectively. The detailed results are summarized in Supporting Information. PB2TCl-*o* based devices can generate high hole and electron mobilities of 1.08×10^{-4} and 1.32×10^{-4} cm^2 V^{-1} s^{-1}, respectively, with a μ_h/μ_e ratio of 0.82. In comparison, it is quite difficult to obtain the $J^{1/2}$–V curve of PB2TCl-*i* based devices due to the poor charge transport mobilities. The much higher and more balanced hole and electron mobilities of PB2TCl-*o* based devices can well explain the excellent J_{sc} and FF values. The steady state photoluminescence (PL) is also measured to understand the charge transfer between donor and acceptor. As shown in Figure S3c (Supporting Information), the emission of PB2TCl-*o*:BTP-ec9-4F blend film at 930 nm is almost completely quenched, as a contrast, PB2TCl-*i*:BTP-ec9-4F blend film still display a strong PL intensity. This result indicates there is an efficient hole transfer from BTP-ec9-4F to PB2TCl-*o*. Besides, the external quantum efficiency of electroluminescence (EQE_{EL}) of OSCs based on PB2TCl-*o*:BTP-ec9-4F is also measured (Supporting Information). The nonradiative energy loss (ΔV_{nr}) can be calculated from the EQE_{EL} by the equation: $q\Delta V_{nr} = -kT\ln(EQE_{EL})$. PB2TCl-*o*-based device gives a ΔV_{nr} of about 0.15 eV, which is among the smallest ΔV_{nr}s of devices over 15%.[36–39]

Furthermore, PB2TCl-*o*:BTP-ec9-4F active layer displays a good transmittance, which can be used to prepare semitransparent OSCs with a device structure of ITO/PEDOT:PSS (30 nm)/PB2TCl-*o*:BTP-ec9-4F (100 nm)/PDINN/Ag (15 or 25 nm), and the results are summarized in **Table 3**. The transmittance of active layer and semitransparent OSCs is also investigated, average visible transmittance (AVT) (370–740 nm) and average transmittance (AT) (400–600 nm) are two key parameters to estimate the features,[40–44] which can be adjusted by the thickness of Ag electrode. As shown in Figure 3c,d,

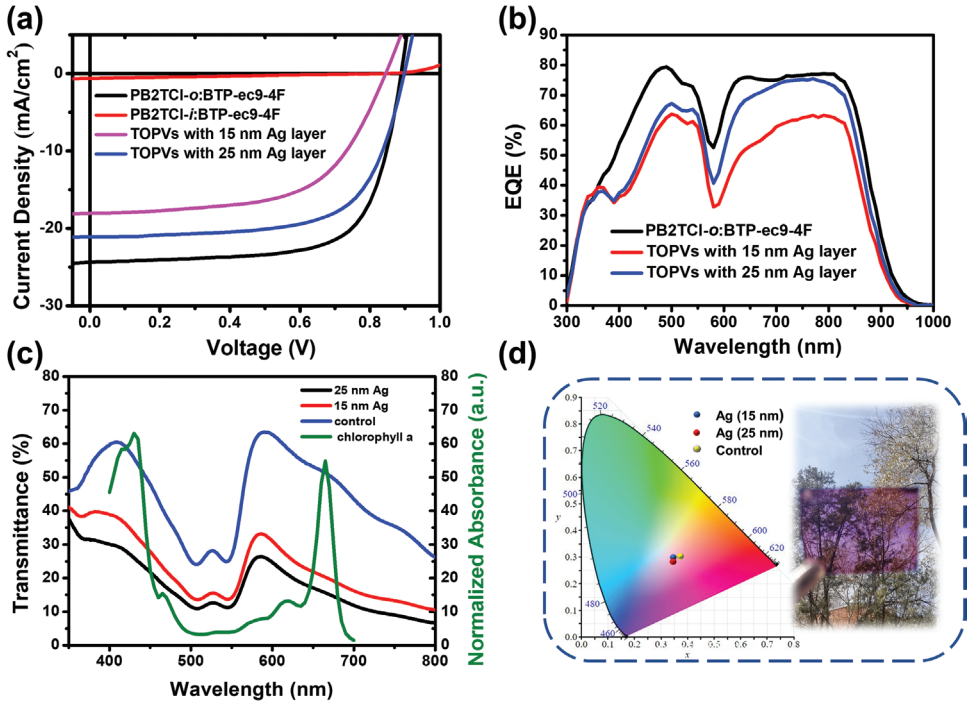

Figure 3. a) *J*–*V* and b) EQEs curves; c) transmission spectra of semitransparent OSCs; d) color coordinates with different anode thicknesses on the CIE 1931 chromaticity diagram and photograph of semitransparent OSCs without Ag electrode.

Table 3. Photovoltaic and transmittance parameters of semitransparent devices based on PB2TCl-*o*.

Ag thickness [nm]	V_{oc} [V]	J_{sc} [mA cm^{-2}]	FF [%]	$PCE_{max/ave}$ [%]	AVT [%]	AT [%]
15	0.84	18.04 (17.57)[a)]	59.66	9.09 (8.81)	23.9	24.2
25	0.89	21.09 (20.71)[a)]	66.46	12.48 (11.95)	18.7	19.2

[a)]Calculated by EQE curve.

OSCs with 15 nm Ag electrode can generate a PCE of 9.09%, with an AVT of 23.9%, an AT of 24.2% and chromaticity coordinates of CIE (0.353, 0.290); and the device with 25 nm Ag electrode can afford a PCE of 12.58%, with an AVT of 18.7%, an AT of 19.2%, chromaticity coordinates of CIE (0.354, 0.294). A photograph of semitransparent OSC without Ag electrode is also shown in Figure 3d. Besides, the absorption of chlorophyll a for plant growth (400–450 and 650–700 nm)[45] is also illustrated in Figure 3c. Due to the well-controlled absorption range of polymer donor and electron acceptor, the regions of transparence spectra of the PB2TCl-*o* based semitransparent devices coincide with the absorption of chlorophyll a, which can be potentially applied to greenhouse for agricultural applications.

The GIWAXS measurements are performed to investigate the crystalline properties and molecular orientations of the neat and blend films. As shown in **Figure 4**, PB2TCl-*o* and PB2TCl-*i* both adopt "face-on" molecular orientations according to one-dimensional (1D) profiles and two-dimensional (2D) patterns. The (010) diffraction peaks of PB2TCl-*o* and PB2TCl-*i* neat films in the out-of-plane (OOP) direction are located at 1.64 and 1.57 Å^{-1}, corresponding to π–π stacking distances of 3.83 and 4.00 Å, respectively. Compared with PB2TCl-*i* neat film, the smaller π–π stacking distance and stronger (010) diffraction peak intensity of PB2TCl-*o* neat film mean closer π–π stacking and stronger intermolecular interaction, which is consistent with its more planar molecular backbone. As for the blend films, PB2TCl-*o*:BTP-ec9-4F displays only an obvious (010) diffraction peak in OOP direction with a π–π stacking distance of 3.67 Å; whereas PB2TCl-*i*:BTP-ec9-4F exhibits observable two separated peaks, corresponding to the (010) diffraction peaks of donor and acceptor. This phenomenon indicates the formation of large domains of donor and acceptor in the PB2TCl-*i*:BTP-ec9-4F blend film, which is consistent with the morphology investigation result (vide infra).

The morphologies of blend films are investigated by atomic force microscopy (AFM) and transmission electron microscopy (TEM) to gain further insight into the different photovoltaic performance of PB2TCl-*o* and PB2TCl-*i* based devices. As shown in **Figure 5**, PB2TCl-*o* based blend film displays more homogenous phase morphology with a smaller root-mean square roughness value (RMS) value of 0.84 nm; whereas PB2TCl-*i* based blend film exhibits a very large phase separation with a RMS value of 2.47 nm. Moreover, the same tendency can be also observed in TEM images. The large size phase separation for the PB2TCl-*i*:BTP-ec9-4F blend film is probably due to the high solubility of PB2TCl-*i* in the processing solvent, which cannot form fibril networks to prevent the acceptor molecule from forming large size aggregate. Favorable morphology is beneficial for efficient charge transfer/transport in the donor or acceptor phase, which can well explain the high J_{sc} and FF values of PB2TCl-*o*:BTP-ec9-4F based devices.[46]

Due to the poor solubilities of PM6 and D18 in non-halogenated solvents, devices processed by non-halogenated solvents usually display inferior efficiency to those processed by halogenated solvents. As shown in **Table 4**,

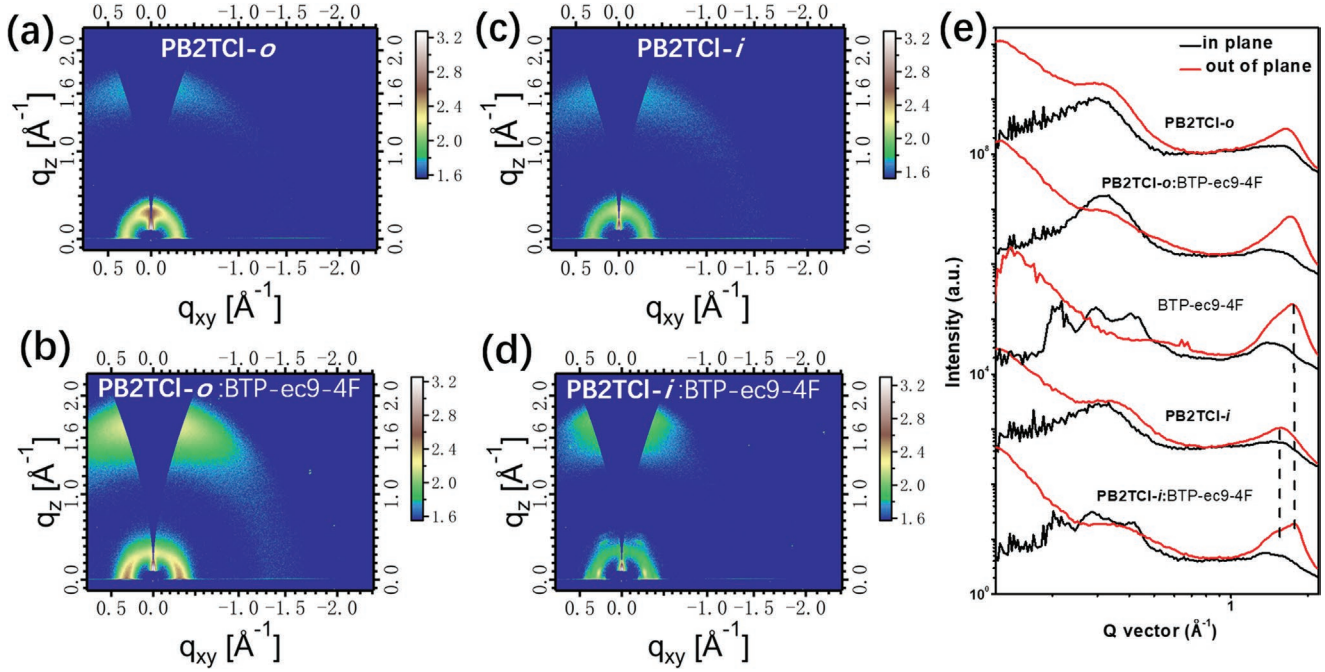

Figure 4. a–d) GIWAXS patterns of the neat/blend films of PB2TCl-*o* and PB2TCl-*i*. e) The corresponding scattering profiles of the neat and blend films.

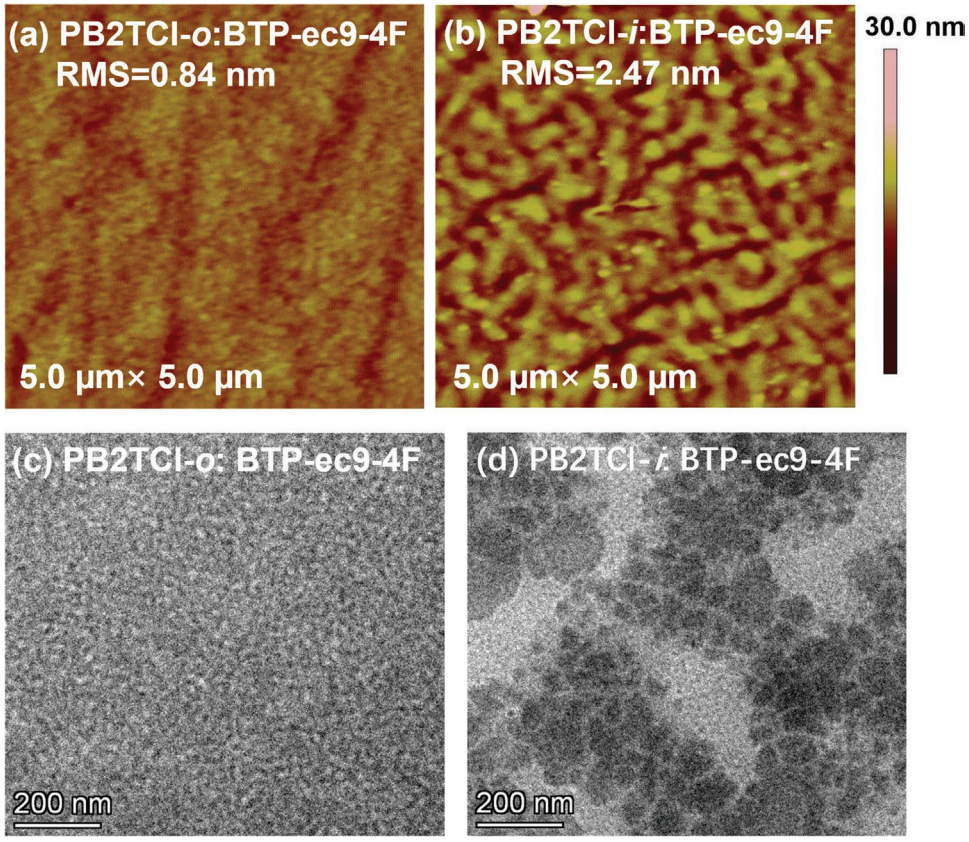

Figure 5. AFM and TEM images of PB2TCl-*o*:BTP-ec9-4F and PB2TCl-*i*:BTP-ec9-4F blend films.

PM6:BTP-ec9-4F and D18:BTP-ec9-4F based non-halogenated solvent processed devices can only give PCEs of 15.16% and 16.18%, respectively. Herein, B2TCl-*o* is used as a building block to prepare random terpolymers PW1 and PW2 (**Scheme 2**). Ternary random copolymerization can usually reduce the crystallinity and improve the solubility of the resulted terpolymers.[47,48] As expected, terpolymers PW1 and PW2 exhibit good solubilities in *o*-DMB. The photovoltaic performance of PW1 and PW2 is also investigated by fabricating inverted devices with a configuration of ITO/PEDOT:PSS/Donor:BTP-ec9-4F/PDINN/Ag. As shown in Table 4, PW1:BTP-ec9-4F and PW2:BTP-ec9-4F based devices give PCEs of 16.26% and 17.19%, respectively, which are higher than the corresponding parent polymers. Moreover, the V_{oc}s of terpolymer based devices are both higher than the corresponding parent polymers based ones. Our results indicate that B2TCl-*o* is a potential versatile building block for designing high-performance non-halogenated solvent processable polymers.

Table 4. Photovoltaic parameters of PW1 and PW2 based devices.

Active layer	V_{oc} [V]	J_{sc} [mA cm^{-2}]	FF [%]	$PCE_{max/ave}$ [%]
PW1:BTP-ec9-4F[a)]	0.86	26.97 (25.62)[b)]	70.45	16.26 (16.13)
PM6:BTP-ec9-4F[a)]	0.82	26.93	68.61	15.16
PW2:BTP-ec9-4F[a)]	0.87	27.32 (26.03)[b)]	72.72	17.19 (16.83)
D18:BTP-ec9-4F[a)]	0.83	26.10	74.95	16.18

[a)]Processed by *o*-DMB; [b)]Calculated by EQE.

3. Conclusion

In this work, two building blocks B2TCl-*o* and B2TCl-*i* with C_{2V} symmetry are designed and used to prepare wide-bandgap polymer donor materials PB2TCl-*o* and PB2TCl-*i*. These two polymers exhibit good solubilities in non-halogenated solvent due to their "zig-zag shape" molecular conformations. Unlike B2TCl-*i*, B2TCl-*o* with two Cl atoms at outer-positions displays nearly planar molecular geometry, which brings significantly difference of PB2TCl-*o* and PB2TCl-*i* in absorption spectra, aggregation behaviors, photovoltaic performances, etc. When blended with low-bandgap acceptor BTP-ec9-4F, PB2TCl-*o* based devices give a PCE of 15.10% with *o*-DMB as the processing solvent; whereas PB2TCl-*i* based devices can only achieve a PCE of 0.13%. Moreover, the semitransparent OSCs based on PB2TCl-*o*:BTP-ec9-4 can also afford a PCE of 9.09% with an AVT of 23.9% and an AT of 24.2%. Furthermore, the building block B2TCl-*o* can be also used to prepare random terpolymer PW1 and PW2 as the third component to reduce the crystallinity and improve the solubility of the terpolymers. Using *o*-DMB as processing solvent, random terpolymers PW1 and PW2 based devices give improved PCEs of 16.26% and 17.19%, respectively, which are much higher than the parent polymers

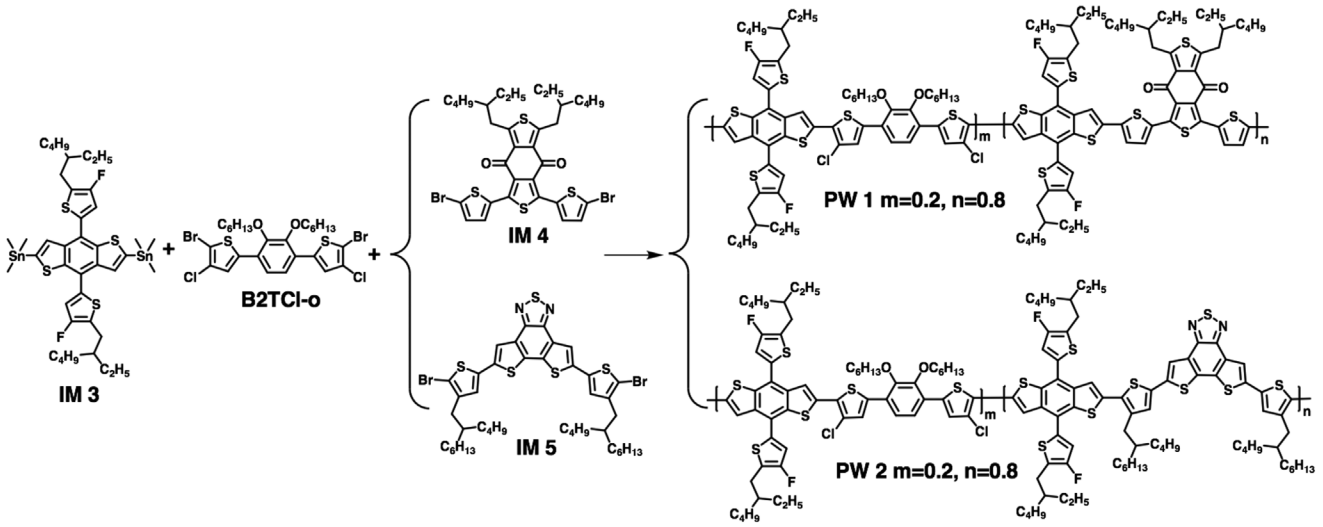

Scheme 2. The chemical structures of random terpolymer PW1 and PW2.

PM6 (15.16%) and D18 (16.18%). Taking into account molecular symmetry and planarity, our work provide a useful molecular design strategy to build high-performance non-halogenated solvent processable polymer donor materials.

Supporting Information

Supporting Information is available from the Wiley Online Library or from the author.

Acknowledgements

H.W. and H.L. contributed equally to this work. This work was financially supported by National Natural Science Foundation of China (51933001, 22109080, 21734009, 52173174).

Conflict of Interest

The authors declare no conflict of interest.

Data Availability Statement

Research data are not shared.

Keywords

C_{2V} symmetry, high-performance, non-halogenated solvents, organic solar cells, semitransparent, terpolymers

Received: December 25, 2021
Revised: February 12, 2022
Published online:

[1] A. J. Heeger, *Adv. Mater.* **2014**, *26*, 10.
[2] Y. Chen, X. Wan, G. Long, *Acc. Chem. Res.* **2013**, *46*, 2645.
[3] Y. Liu, B. Li, C. Q. Ma, F. Huang, G. Feng, H. Chen, J. Hou, L. Yan, Q. Wei, Q. Luo, Q. Bao, W. Ma, W. Liu, W. Li, X. Wan, X. Hu, Y. Han, Y. Li, Y. Zhou, Y. Zou, Y. Chen, Y. Li, Y. Chen, Z. Tang, Z. Hu, Z. Zhang, Z. Bo, *Sci. China: Chem.* **2022**, *64*, 224.
[4] Y. Lin, J. Wang, Z. G. Zhang, H. Bai, Y. Li, D. Zhu, X. Zhan, *Adv. Mater.* **2015**, *27*, 1170.
[5] J. Yuan, Y. Zhang, L. Zhou, G. Zhang, H.-L. Yip, T.-K. Lau, X. Lu, C. Zhu, H. Peng, P. A. Johnson, M. Leclerc, Y. Cao, J. Ulanski, Y. Li, Y. Zou, *Joule* **2019**, *3*, 1140.
[6] L. Wang, C. Guo, X. Zhang, S. Cheng, D. Li, J. Cai, C. Chen, Y. Fu, J. Zhou, H. Qin, D. Liu, T. Wang, *Chem. Mater.* **2021**, *33*, 8854.
[7] C. Li, J. Zhou, J. Song, J. Xu, H. Zhang, X. Zhang, J. Guo, L. Zhu, D. Wei, G. Han, J. Min, Y. Zhang, Z. Xie, Y. Yi, H. Yan, F. Gao, F. Liu, Y. Sun, *Nat. Energy* **2021**, *6*, 605.
[8] H. Meng, C. Liao, M. Deng, X. Xu, L. Yu, Q. Peng, *Angew. Chem., Int. Ed.* **2021**, *60*, 22554.
[9] Y. Cui, Y. Xu, H. Yao, P. Bi, L. Hong, J. Zhang, Y. Zu, T. Zhang, J. Qin, J. Ren, Z. Chen, C. He, X. Hao, Z. Wei, J. Hou, *Adv. Mater.* **2021**, *33*, 2102420.
[10] F. Liu, L. Zhou, W. Liu, Z. Zhou, Q. Yue, W. Zheng, R. Sun, W. Liu, S. Xu, H. Fan, L. Feng, Y. Yi, W. Zhang, X. Zhu, *Adv. Mater.* **2021**, *33*, 2100830.
[11] T. Wang, R. Sun, M. Shi, F. Pan, Z. Hu, F. Huang, Y. Li, J. Min, *Adv. Energy. Mater.* **2020**, *10*, 2000590.
[12] L. Zhan, S. Li, T.-K. Lau, Y. Cui, X. Lu, M. Shi, C.-Z. Li, H. Li, J. Hou, H. Chen, *Energy Environ. Sci.* **2020**, *13*, 635.
[13] K. Gao, Y. Kan, X. Chen, F. Liu, B. Kan, L. Nian, X. Wan, Y. Chen, X. Peng, T. P. Russell, Y. Cao, A. K. Jen, *Adv. Mater.* **2020**, *32*, 1906129.
[14] W. Wang, C. Yan, T. K. Lau, J. Wang, K. Liu, Y. Fan, X. Lu, X. Zhan, *Adv. Mater.* **2017**, *29*, 1701308.
[15] Y. Liu, H. Lu, M. Li, Z. Zhang, S. Feng, X. Xu, Y. Wu, Z. Bo, *Macromolecules* **2018**, *51*, 8646.
[16] S. Lee, D. Jeong, C. Kim, C. Lee, H. Kang, H. Y. Woo, B. J. Kim, *ACS Nano* **2020**, *14*, 14493.
[17] X. Xu, G. Zhang, L. Yu, R. Li, Q. Peng, *Adv. Mater.* **2019**, *31*, 1906045.
[18] R. K. Henderson, C. Jiménez-González, D. J. C. Constable, S. R. Alston, G. G. A. Inglis, G. Fisher, J. Sherwood, S. P. Binks, A. D. Curzons, *Green Chem.* **2011**, *13*, 854.
[19] D. Wang, G. Zhou, Y. Li, K. Yan, L. Zhan, H. Zhu, X. Lu, H. Chen, C. Z. Li, *Adv. Funct. Mater.* **2021**, *32*, 2107827.
[20] X. Xu, L. Yu, H. Yan, R. Li, Q. Peng, *Energy Environ. Sci.* **2020**, *13*, 4381.

[21] Y. Huang, E. J. Kramer, A. J. Heeger, G. C. Bazan, *Chem. Rev.* **2014**, *114*, 7006.
[22] Z. Wang, K. Gao, Y. Kan, M. Zhang, C. Qiu, L. Zhu, Z. Zhao, X. Peng, W. Feng, Z. Qian, X. Gu, A. K. Jen, B. Z. Tang, Y. Cao, Y. Zhang, F. Liu, *Nat. Commun.* **2021**, *12*, 332.
[23] J. J. van Franeker, G. H. Heintges, C. Schaefer, G. Portale, W. Li, M. M. Wienk, P. van der Schoot, R. A. Janssen, *J. Am. Chem. Soc.* **2015**, *137*, 11783.
[24] S. E. Shaheen, C. J. Brabec, N. S. Sariciftci, F. Padinger, T. Fromherz, J. C. Hummelen, *Appl. Phys. Lett.* **2001**, *78*, 841.
[25] J. Zhao, Y. Li, G. Yang, K. Jiang, H. Lin, H. Ade, W. Ma, H. Yan, *Nat. Energy* **2016**, *1*, 15027.
[26] Z. Li, L. Ying, P. Zhu, W. Zhong, N. Li, F. Liu, F. Huang, Y. Cao, *Energy Environ. Sci.* **2019**, *12*, 157.
[27] Y. Qin, L. Ye, S. Zhang, J. Zhu, B. Yang, H. Ade, J. Hou, *J. Mater. Chem. A* **2018**, *6*, 4324.
[28] K. Wang, W. Li, X. Guo, Q. Zhu, Q. Fan, Q. Guo, W. Ma, M. Zhang, *Chem. Mater.* **2021**, *33*, 5981.
[29] H. Lu, P. Jiang, Y. Wei, S. Yuan, Y. Liu, W. Li, X. Xu, Z. Bo, *Sol. RRL* **2020**, *4*, 2000547.
[30] T. Liu, X. Pan, X. Meng, Y. Liu, D. Wei, W. Ma, L. Huo, X. Sun, T. H. Lee, M. Huang, H. Choi, J. Y. Kim, W. C. Choy, Y. Sun, *Adv. Mater.* **2017**, *29*, 1604251.
[31] H. Wang, H. Lu, Y. N. Chen, G. Ran, A. Zhang, D. Li, N. Yu, Z. Zhang, Y. Liu, X. Xu, W. Zhang, Q. Bao, Z. Tang, Z. Bo, *Adv. Mater.* **2021**, *2021*, 2105483.
[32] R. Hou, M. Li, X. Ma, H. Huang, H. Lu, Q. Jia, Y. Liu, X. Xu, H. B. Li, Z. Bo, *ACS Appl. Mater. Interfaces* **2020**, *12*, 46220.
[33] Z. Li, K. Jiang, G. Yang, J. Y. Lai, T. Ma, J. Zhao, W. Ma, H. Yan, *Nat. Commun.* **2016**, *7*, 13094.
[34] Y. Cui, H. Yao, J. Zhang, K. Xian, T. Zhang, L. Hong, Y. Wang, Y. Xu, K. Ma, C. An, C. He, Z. Wei, F. Gao, J. Hou, *Adv. Mater.* **2020**, *32*, 1908205.
[35] T. Wang, J. Qin, Z. Xiao, J. Zhang, Z. Chen, L. Zhang, M. Cheng, Z. Jin, Y. Yuan, W.-Q. Wu, C. Duan, S. Xie, K. Sun, F. Hao, L. Ding, *Nano Energy* **2020**, *77*, 105161.
[36] S. Liu, J. Yuan, W. Deng, M. Luo, Y. Xie, Q. Liang, Y. Zou, Z. He, H. Wu, Y. Cao, *Nat. Photonics* **2020**, *14*, 300.
[37] Y. Shi, J. Pan, J. Yu, J. Zhang, F. Gao, K. Lu, Z. Wei, *Sol. RRL* **2021**, *5*, 2100008.
[38] C. Sun, F. Pan, S. Chen, R. Wang, R. Sun, Z. Shang, B. Qiu, J. Min, M. Lv, L. Meng, C. Zhang, M. Xiao, C. Yang, Y. Li, *Adv. Mater.* **2019**, *31*, 1905480.
[39] Y. Tang, J. Yu, H. Sun, Z. Wu, C. W. Koh, X. Wu, B. Liu, J. Wang, Q. Liao, Y. Li, H. Guo, H. Y. Woo, F. Gao, X. Guo, *Sol. RRL* **2020**, *4*, 2000396.
[40] K.-S. Chen, J.-F. Salinas, H.-L. Yip, L. Huo, J. Hou, A. K. Y. Jen, *Energy Environ. Sci.* **2012**, *5*, 9551.
[41] Y. Liu, P. Cheng, T. Li, R. Wang, Y. Li, S. Y. Chang, Y. Zhu, H. W. Cheng, K. H. Wei, X. Zhan, B. Sun, Y. Yang, *ACS Nano* **2019**, *13*, 1071.
[42] P. Yin, Z. Yin, Y. Ma, Q. Zheng, *Energy Environ. Sci.* **2020**, *13*, 5177.
[43] S. Chen, H. Yao, B. Hu, G. Zhang, L. Arunagiri, L. K. Ma, J. Huang, J. Zhang, Z. Zhu, F. Bai, W. Ma, H. Yan, *Adv. Energy Mater.* **2018**, *8*, 1800529.
[44] D. Wang, R. Qin, G. Zhou, X. Li, R. Xia, Y. Li, L. Zhan, H. Zhu, X. Lu, H. L. Yip, H. Chen, C. Z. Li, *Adv. Mater.* **2020**, *32*, 2001621.
[45] S.-Y. Chang, P. Cheng, G. Li, Y. Yang, *Joule* **2018**, *2*, 1039.
[46] K. Gao, J. Miao, L. Xiao, W. Deng, Y. Kan, T. Liang, C. Wang, F. Huang, J. Peng, Y. Cao, F. Liu, T. P. Russell, H. Wu, X. Peng, *Adv. Mater.* **2016**, *28*, 4727.
[47] J. Lee, S. M. Lee, S. Chen, T. Kumari, S. H. Kang, Y. Cho, C. Yang, *Adv. Mater.* **2019**, *31*, 1804762.
[48] X. Li, G. Huang, H. Wang, T. Wang, Z. Zhao, H. Peng, C. Cao, Y. Qi, W. Chen, R. Yang, *Chem. Eng. J.* **2021**, *422*, 130097.